Statistical Model for Diffusion Attenuated MR Signal

Dmitriy A. Yablonskiy,[1,2*] G. Larry Bretthorst,[1] and Joseph J.H. Ackerman[1,3,4]

A general statistical model that can describe a rather large number of experimental results related to the structure of the diffusion-attenuated MR signal in biological systems is introduced. The theoretical framework relies on a phenomenological model that introduces a distribution function for tissue apparent diffusion coefficients (*ADC*). It is shown that at least two parameters—the position of distribution maxima (*ADC*) and the distribution width (σ)—are needed to describe the MR signal in most regions of a human brain. A substantial distribution width, on the order of 36% of the *ADC*, was found for practically all brain regions examined. This method of modeling the MR diffusion measurement allows determination of an intrinsic tissue-specific *ADC* for a given diffusion time independent of the strength of diffusion sensitizing gradients. The model accounts for the previously found biexponential behavior of the diffusion-attenuated MR signal in CNS. Magn Reson Med 50:664–669, 2003.

Key words: diffusion; magnetic resonance; MRI; MRS; CNS

Growing interest in diffusion MRI stems from numerous clinical and research applications (for example, see recent reviews in special issues of NMR in Biomedicine (1,2)). Most applications rely on a Stejskal-Tanner (3) pulsed gradient spin echo (PGSE) experiment and an assumption that the diffusion-attenuated MR signal can be expressed as a monoexponential function given by (3):

$$S = S_0 \exp(-b\,ADC). \qquad [1]$$

Here *ADC* is the apparent diffusion coefficient for tissue-water or other MR active species under consideration; the so-called *b*-value depends on the shape of the diffusion-sensitizing gradient pulse waveform $G(t)$ (4):

$$b = \gamma^2 \int_0^t dt' \left[\int_0^{t'} dt''\ G(t'') \right]^2, \qquad [2]$$

where γ is the magnetogyric (late gyromagnetic) ratio of the nuclide under consideration. For example (3), for the case of bipolar rectangular gradient pulses with amplitude G, duration δ and interval between pulse centers Δ:

$$b = (\gamma G \delta)^2 \left(\Delta - \frac{1}{3}\,\delta \right). \qquad [3]$$

However, numerous studies of the diffusion of water and/or other metabolites in brain tissue and other biological systems have documented a non-monoexponential behavior of the MR signal S as a function of the *b*-value at fixed diffusion times (e.g., see Refs. 5–17). Most authors report that their data can be fit well by a biexponential function with two different diffusion coefficients (large/fast and small/slow) and suggest ascribing the two exponential components to two physical compartments (extra- and intracellular) in a tissue. However, as noted by Le Bihan and van Zijl (18), the origin of fast- and slow-diffusion pools is "still mysterious." Moreover, Sehy et al. (19) have directly observed biexponential diffusion MR signal behavior within the intracellular space of a single cell, the frog oocyte.

Generally speaking, Eqs. [1] and [3] describe the diffusion-attenuated MR signal in a PGSE experiment only for unrestricted diffusion in homogeneous media. However, in most in vivo experiments each imaging or spectroscopic voxel contains numerous cells with different cell types, sizes, geometries, orientations, membrane permeabilities, and presumably different T_2 and T_1 relaxation time constants. Hence, the expectation that such a system can be described in terms of a simple unrestricted diffusion (monoexponential) model Eq. [1] is not reasonable. Practically any of the above-mentioned issues can lead to a deviation from monoexponential behavior—a point clearly illustrated in a recent article by Chin et al. (20). These authors carried out numerical simulations for a realistic geometrical structure of a rat spinal cord and found that under a variety of conditions the signal behavior is not monoexponential and can be generally described in terms of biexponential diffusion attenuation. Theoretical modeling of diffusion in multicompartment systems with cylindrical geometry by van der Weerd et al. (21) also demonstrated that "multi-exponential analysis of diffusion signal behavior cannot be freely related to the geometrical parameters of the system." Moreover, for short diffusion times this laboratory has shown that biexponential signal behavior is predicted theoretically even for a single homogeneous compartment (22). A number of theoretical models based on the complex structure of biological objects have also been developed to describe non-monoexponential PGSE MR signal behavior (10,16, 23–27,32). While in some cases a biexponential behavior of an MR signal can obviously be related to the tissue compartmentalization or geometrical structure, in most cases it simply reflects the fact that a biexponential function describes signal behavior better than does a monoexponential function without a simple obvious relationship between the biexponential model's parameters and the physical parameters of the system under investigation.

[1]Department of Radiology, Washington University School of Medicine, St. Louis, Missouri.

[2]Department of Physics, Washington University, St. Louis, Missouri.

[3]Department of Chemistry, Washington University, St. Louis, Missouri.

[4]Department of Medicine, Washington University School of Medicine, St. Louis, Missouri.

Grant sponsor: NIH; Grant numbers: R01 NS4519-01A1; R01 HL70037; R24 CA83060.

*Correspondence to: Dmitriy A. Yablonskiy, Ph.D., Mallinckrodt Institute of Radiology, 4525 Scott Ave., St. Louis, MO 63110.
E-mail: YablonskiyD@mir.wustl.edu

Received 25 March 2003; revised 28 May 2003; accepted 10 June 2003.

DOI 10.1002/mrm.10578
Published online in Wiley InterScience (www.interscience.wiley.com).

It would seem reasonable to develop a well-defined physical model that recognizes the presence of variable length scales for restrictions and hindrances to water diffusion in biological systems. Such systems, which by their very nature represent highly complicated structures, present an architectural arrangement characterized by an extraordinary range of length scales. The MR diffusion experiment is sensitive to a subset of the full range of possible length scales, dependent on experimental parameters and the practical constraints of the measurement (SNR, etc.). The MR relevant range of length scales for restrictions and hindrances to water diffusion should be reflected in any model of MR diffusion data from biological systems. The critical issue is how best to do this. Below we propose a statistical method/model to reflect in a well-defined manner the consequences of a distribution of length scales for restrictions and hindrances to water diffusion (i.e., by a resulting diffusion coefficient probability distribution characterized by a mean value and a distribution width). This general phenomenological model can describe a rather large number of experimental results related to the structure of PGSE diffusion-attenuated MR signal in biological systems. We apply this model to describe MR data in a human brain and demonstrate good agreement with data obtained from practically all regions of brain for a *b*-value interval from zero to 2 ms/μm^2.

THEORETICAL MODEL

Assumptions

1. The MR signal from a given voxel containing a variety of cells, and intercellular and extracellular spaces, can be described as a sum of signals from a large number of individual spin packets originating from different positions within the voxel.
2. Each spin packet has its own *ADC* and contributes to the signal as described in Eq. [1].
3. Because spin packets originate from different positions, travel through different displacement trajectories, and are confronted with different restrictions and hindrances to displacement, their *ADCs* are, generally speaking, different.
4. The total MR signal can be described in terms of a distribution function *P(ADC)* that gives the fraction of spin packets with a given *ADC*.
5. Generally speaking, both *ADC* and *P(ADC)*, for a given spin packet, depend on the pulse gradient waveform structure (gradient strength, direction, duration, shape and diffusion time). For the sake of simplicity, we will keep these dependences in mind but will omit them in the notation. For compactness we will sometimes also use the notation *D* instead of *ADC*.

Under these conditions, the MR signal can be written as:

$$S = S_0 \int_0^\infty dD\, P(D)\exp(-b\,D). \qquad [4]$$

For the limiting case of free diffusion characterized by a diffusion coefficient D_0, the distribution function is a delta function:

$$P_0(D) = \delta(D - D_0). \qquad [5]$$

and the MR signal reduces to a monoexponential, Eq. [1], with $ADC = D_0$. If a voxel were to contain several identifiable pools with MR-weighted population fractions f_i and apparent diffusion coefficients ADC_i (both sequence dependent) the distribution function is:

$$P(D) = \sum f_i\, \delta(D - ADC_i), \qquad [6]$$

and the signal is a sum of weighted monoexponentials:

$$S = S_0 \sum f_i \exp(-b\, ADC_i). \qquad [7]$$

However, as noted earlier, biological tissue possesses an exceedingly complex structural microarchitecture and postulating a small number of identifiable pools to describe water displacement would seem counterintuitive. Indeed, it is far more likely that each of the large number of spin packets within a voxel experiences a net displacement somewhat different from all the other spin packets. The issue before us is how to express this global physical model in mathematical form. In the case of signal from CNS, if the diffusion time Δ is much longer than the characteristic time required for molecules to encounter a multitude of hindrances and restrictions to displacement, then most spin packets can be expected to sample similar displacement trajectories and environments. This physical model results in a peak-shaped distribution function, *P(D)*. The exact shape depends on the details of the structural microarchitecture within the voxel. However, under a realistic assumption that a large number of "similar" cells reside in a voxel, the width of the distribution should be rather small and the "tails" of the distribution should decay rather fast. Obviously, these assumptions can be satisfied by a Gaussian-type function:

$$P(D) = A\, \exp[-(D - ADC)^2/2\sigma^2] \quad \text{for} \quad D > 0,$$
$$\text{and} \quad P(D) = 0 \quad \text{for} \quad D < 0. \qquad [8]$$

In this equation, A is a normalization constant:

$$A^{-1} = \int_0^\infty \exp[-(D - ADC)^2/2\sigma^2]$$
$$= \sigma\sqrt{\pi/2}\left[1 + \Phi\left(\frac{ADC}{\sigma\sqrt{2}}\right)\right], \qquad [9]$$

ADC now corresponds to the position of the distribution maximum (peak), σ is the width of the distribution, and Φ is the error function.

Substitution of Eqs. [8] and [9] in Eq. [4] gives:

$$S = S_0\, F;$$

$$F = \frac{1 + \Phi\left(\dfrac{ADC}{\sigma\sqrt{2}} - \dfrac{b\sigma}{\sqrt{2}}\right)}{1 + \Phi\left(\dfrac{ADC}{\sigma\sqrt{2}}\right)} \exp\left(-b\, ADC + \frac{1}{2}\, b^2\sigma^2\right) \qquad [10]$$

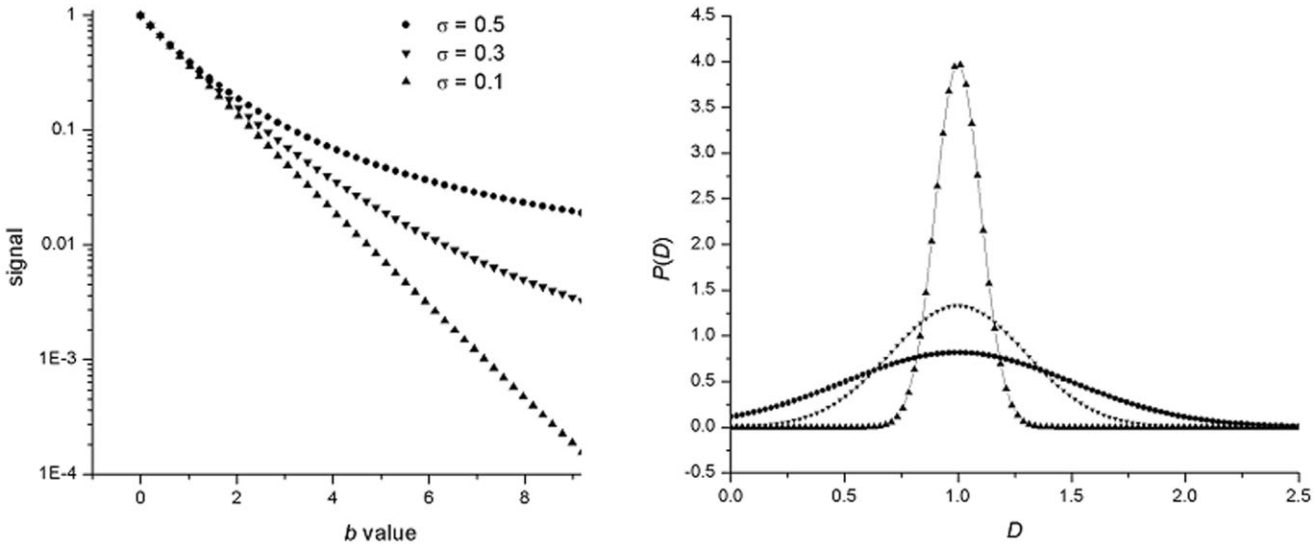

FIG. 1. Diffusion attenuated MR signal (Eq. [10]) (left) and corresponding Gaussian-type distribution functions (Eq. [8]) (right). Data are shown for *ADC* = 1 and different distribution widths σ. For small σ, deviation of the signal from mono-exponential behavior is hardly visible. Though it becomes very pronounced for large σ.

For very small *b*-values, Eq. [10] reduces to a monoexponential function (Eq. [1]); however, as *b* grows, the decay rate becomes slower due to the positive term $b^2\sigma^2/2$. Nevertheless, the positive term $b^2\sigma^2/2$ never leads to signal growth because it is compensated for by a similar negative term in the preexponential error function. For large *b*-values, Eq. [10] decays as $1/b$:

$$S \rightarrow S_0 \left[\frac{\sqrt{2/\pi}\, \exp(-ADC^2/2\sigma^2)}{1 + \Phi(ADC/\sigma\sqrt{2})} \right] \frac{1}{b\,\sigma - ADC/\sigma}. \quad [11]$$

Examples of distribution functions (8) and signal behavior from Eq. [10] are shown in Fig. 1.

In case of unrestricted diffusion, σ tends to zero and the distribution function *P(D)* (8) tends to delta function (5), reducing the signal (10) to Eq. [1]. This feature is demonstrated in Fig. 1. If the distribution width σ is much smaller than the *ADC* (position of distribution maxima) and the *b*-value is much smaller than ADC/σ^2, the signal in Eq. [10] takes a simple form:

$$S = S_0 \exp\left(-b\,ADC + \frac{1}{2}\sigma^2 b^2\right). \quad [12]$$

MATERIALS AND METHODS

Data were obtained on a whole-body 1.5 T Siemens Magnetom Sonata. Human study was approved by the institutional review board. Fifteen axial 2D spin echo EPI images with b = 0.15, 0.3, …, 2.25 ms/μm^2 were taken for each direction of diffusion-sensitizing gradients. Three orthogonal sets of diffusion-sensitizing gradients (along the slice direction, along read-out and phase-encoding directions) were applied. Other sequence parameters were: δ = 35 ms, Δ = 40 ms, slice thickness 6 mm, FOV 256 mm, matrix 128 × 128, TE = 130 ms, TR = 2 sec, number of averages 32. Two adult healthy volunteers were studied. Data were analyzed using Bayesian probability theory to estimate the model parameters for the signal intensity (magnitude images) on a pixel-by-pixel basis. To account for noise in magnitude images, the magnitude of the noise was incorporated into the theoretical model (Eq. [10]) in a standard manner:

$$S = \sqrt{S_0^2 F^2 + n^2}. \quad [13]$$

The noise magnitude *n* in Eq. [13] was estimated as a mean value in the image background. In the examples shown herein, *n* was 12.5. However, setting *n* to zero had very little effect on parameter estimation except in regions with very high diffusivity as, for example, in CSF or white matter tracks when diffusion-sensitizing gradients were applied parallel to the tract directions.

The method was first validated on a water phantom where a delta-function distribution (Eq. [5]) is expected. The *ADC* and σ maps are shown in Fig. 2. Indeed, the

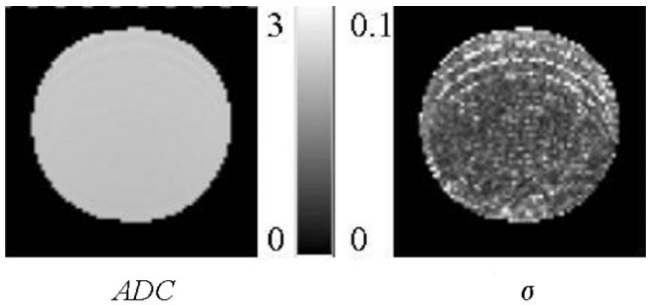

FIG. 2. Maps of *ADC* and σ obtained from a water phantom (room temperature). *ADC* = 2.24 ± 0.03 μm^2/ms (mean ± std), σ = 0.04 ± 0.02 μm^2/ms. Note that even in the area of artifacts visible in the σ map, σ does not exceed 0.1 μm^2/ms. The scale bars provide references for *ADC* (from 0 to 3 μm^2/ms) and σ (from 0 to 0.1 μm^2/ms).

average σ in the distribution width map was 0.04 μm^2/ms, which corresponds to 1.8% of *ADC*.

RESULTS

Examples of data from different brain regions are shown in Fig. 3, along with corresponding fits. Data from all brain tissues (except for CSF in ventricles) show substantial nonlinear diffusion attenuation. Examples of maps of *ADC* and the distribution width σ obtained from the head of one volunteer are shown in Fig. 4. The brightest regions in the *ADC* map correspond to CSF in ventricles and subarachnoid spaces. In the σ map, CSF in ventricles is dark but remains bright at the ventricular edges and in subarachnoid spaces. The latter is most likely due to the partial volume effect (presence of tissue and CSF that have substantially different *ADC*s in the same voxel) that leads to artificial distribution function broadening.

Some of the results for *ADC* and σ obtained from one volunteer are summarized in Fig. 5. They are similar to the data obtained for another volunteer, although some differences exist, most likely due to the relative orientation of field gradients and head position. The average *ADC* across all ROIs for one volunteer was 0.90 ± 0.27 μm^2/ms and the average σ was 0.31 ± 0.07 μm^2/ms or 36 ± 9% if calculated on a per voxel basis as a percentage of corresponding *ADC*. The corresponding numbers for the second volunteer were *ADC*: 0.84 ± 0.20 μm^2/ms, σ: 0.29 ± 0.07 μm^2/ms or 36 ± 9% if calculated as a percentage of corresponding *ADC*.

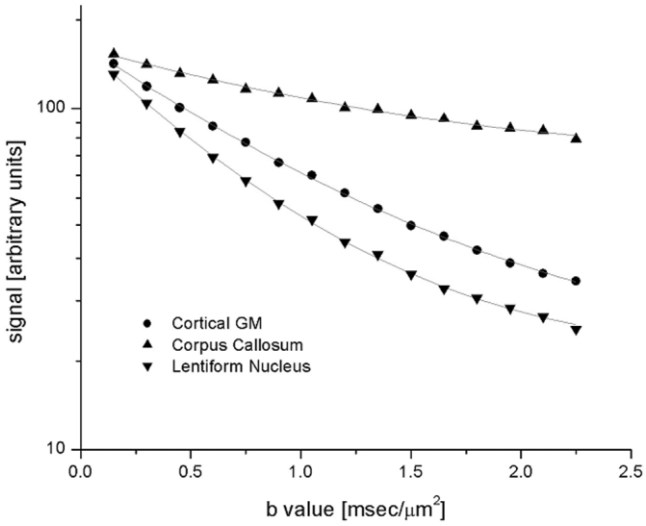

FIG. 3. Examples of data (solid symbols) from representative ROIs and the statistical model with optimally estimated parameters (solid lines) are shown plotted on a semi-logarithmic scale. For all shown data R^2 is higher than 0.99. The nonlinear behavior of MR signal is obvious in all three examples.

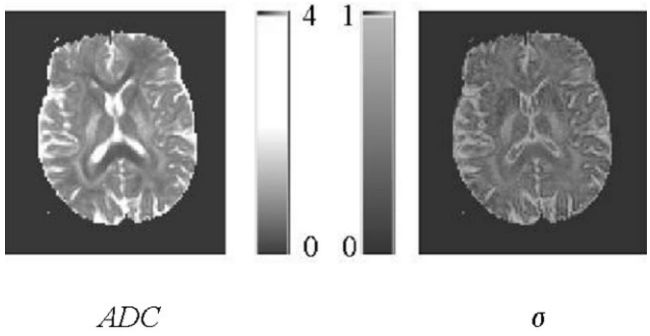

FIG. 4. An example of *ADC* and σ maps corresponding to diffusion sensitizing gradient direction perpendicular to slice orientation. The scale bars provide references for *ADC* (from 0 to 4 μm^2/ms) and σ (from 0 to 1 μm^2/ms).

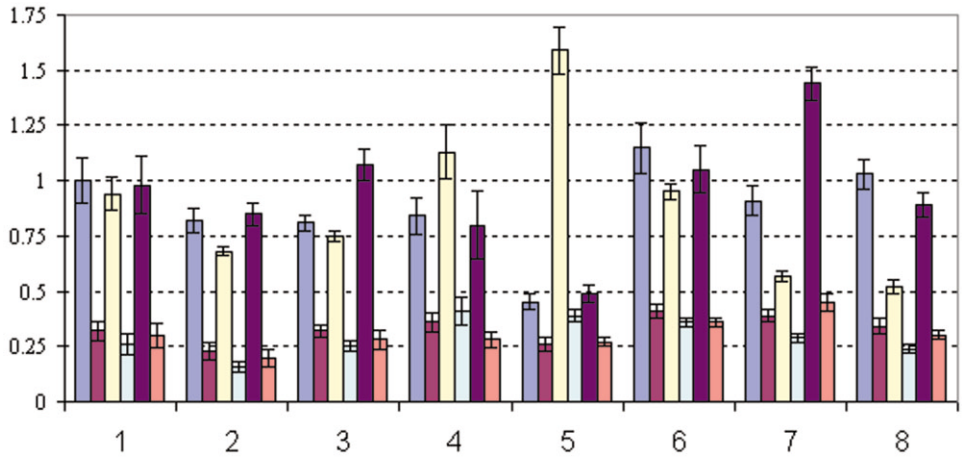

FIG. 5. Data obtained from one volunteer. Columns represent *ADC* and σ pairs in three different directions. The units shown are μm^2/ms. Results are grouped in eight blocks each representing one ROI: 1—frontal GM, 2—head of caudate nucleus, 3—thalamus, 4—occipital-temporal GM, 5—splenium of corpus callosum, 6—occipital WM, 7—frontal WM, 8—external capsule. In each block the first and second columns represent *ADC* and σ corresponding to diffusion perpendicular to slice; the third and fourth columns represent *ADC* and σ corresponding to diffusion in read-out direction (horizontal in Fig. 4). The fifth and sixth columns represent *ADC* and σ corresponding to diffusion in phase-encoding direction (vertical in Fig. 4). Error bars represent variability across ROI, usually about 10 voxels in size. ROIs are selected according to Shimony et al. (31).

DISCUSSION

We have demonstrated that, for practically all human brain regions, the diffusion attenuated MR signal shows non-monoexponential behavior that can be quantified in terms of a statistical model with a Gaussian-type distribution function (Eq. [8]). In this model, the peak position of the Gaussian distribution corresponds to the *ADC*, with values close to those determined previously by standard MR diffusion methods. We also found with the long diffusion time employed herein ($\Delta \sim 40$ ms) that the distribution width σ was relatively constant across different brain tissues in both absolute units (about 0.3 $\mu m^2/ms$) and relative to *ADC* units (about 36%).

It is important to emphasize that our approach, based on fitting the theoretical model (Eq. [10]) (or simplified version (12) for narrow distributions) to the experimental data allows measurement of an intrinsic tissue-specific *ADC* which is independent of the strength of diffusion-sensitizing gradients. At the same time, conventional methods based on a two-*b*-value measurement and assumption of monoexponential behavior inevitably define an *ADC* that is a function of gradient strength. For narrow distributions our theory predicts, from Eq. [12]:

$$ADC(b) = ADC - 0.5\sigma^2 b. \qquad [14]$$

Hence, these conventional two-*b*-value approaches usually measured *ADC*s that are smaller/slower than actual intrinsic *ADC*s. However, for measurements done with typical clinical scanners at an upper *b*-value of 1 $ms/\mu m^2$ and long diffusion times, the difference is modest, about 5%. Such differences may be important, however, for measurements with large *b*-values and especially for quantitative comparisons of data obtained with different approaches or where long term temporal assessment is desired. Because the *ADC* depends on tissue temperature, it may also be important for accurate monitoring of changes in a tissue temperature during functional activation (28). Note, however, that more accurate expression for *ADC* based on Eq. [10] should be used for large *b*-values instead of Eq. [14].

For very large *b*-values, a major contribution to the signal comes from slowly diffusing spin packets. If physical consideration of the object under consideration precludes the presence of spin packets with zero diffusivities, special care should be taken with regard to the behavior of the distribution function at small *D* because the Gaussian distribution Eq. [8] has a nonzero value at $D = 0$. For example, alternative distribution functions:

$$P_n(D) = A_n D^n \exp[-(D - D_n)^2/2\sigma_n^2],$$

$$D_n = ADC - n\sigma_n^2/ADC \qquad [15]$$

can be used to address this issue. However, for a typical σ of about 36% of *ADC*, which we found in a human brain, *P(D)* reduces rapidly and for small *D* is proportional to $\exp(-0.5\ ADC^2/\sigma^2) = 0.02$.

As discussed in the Introduction, a number of articles report that a biexponential diffusion attenuation function describes experimental MR data reasonably well (5–17). It is interesting from this perspective to investigate how our statistical model compares with a biexponential equation. Table 1 is the result of biexponential fitting to synthetic data generated using Eq. [10] with different distribution widths σ. The fits are remarkably good. One can see that the volume fractions of the "two compartments" do not change substantially when distribution width σ is varied. The result that the "fast" component has a "population fraction" of 70–80% is in agreement with previous experimental findings in the above-mentioned articles. Note also that according to Table 1, the diffusivity of the "fast" component remains practically constant, while the diffusivity of the "slow" component decreases with increasing σ. The results in Table 1 are obtained by fitting in the interval $0 \le b\ ADC \le 10$; they could be different if another interval were used.

Because only unrestricted diffusion in a homogeneous medium results in a truly monoexponential signal behavior (Eq. [1]), biophysical mechanisms leading to non-monoexponential behavior are numerous (16,23–27,32). First and foremost are cellular membranes which restrict molecular motion (29,30). Then come intra- and intercellular heterogeneities, which result in heterogeneous distribution of T_1 and T_2 relaxation time constants, spin density, and molecular diffusivities (see, for example, modeling of these effects in Ref. 20). Also, an important contribution may result from a directional microdistribution of elongated cells, such as dendrites in CNS, which produce effects similar to previously described effects for diffusion of hyperpolarized ^{3}He gas in acinar airways of lung (27).

Our approach has the potential to improve MR diffusion-based fiber-tracking techniques. Indeed, in the area of fiber crossing or branching, the distribution function *P(ADC)* is also expected to branch for certain directions of diffusion-sensitizing gradients. This can manifest itself as an increase in the distribution width σ. This effect may provide additional important information on the structure of fibers in a voxel.

Finally, this procedure may prove of value in monitoring and assessing tissue abnormalities and the temporal changes therein such as, for example, brain mechanical and ischemic injuries, white matter diseases, and cancerous tumors undergoing treatment. Diffusion MR has been suggested to provide an early response indicator (see, for example, review articles in Ref. 2) and the theoretical framework presented herein may put the analysis of such changes on firmer footing.

Table 1
Estimated Parameters of Biexponential Fit to a Signal Generated Using Model in Eq. [12]

σ	f1	f2	D1	D2
0.2	0.71	0.29	1.12	0.71
0.3	0.81	0.19	1.11	0.47
0.4	0.83	0.17	1.11	0.32
0.5	0.82	0.18	1.14	0.25

The parameter *ADC* was assumed to be equal to 1 and fitting was performed in the interval $0 \le b\ ADC \le 10$. For all fitted curves $R^2 = 0.9999$.

CONCLUSION

We have provided a framework for analysis of diffusion-attenuated MR signal formation in complex biological systems. Our approach relies on a statistical model that introduces a distribution function for tissue *ADC*. We have demonstrated that at least two parameters—position of the distribution maximum (corresponding to tissue intrinsic *ADC*) and the distribution width σ—are needed for each direction of the diffusion-sensitizing gradients to quantify diffusion in homogeneous biological tissue. This framework allows measurement of intrinsic tissue-specific *ADC* for a given diffusion time independent of the strength of diffusion-sensitizing gradients. The method was applied to a study of a human brain where for diffusion times ~40 ms, we found a substantial distribution width on the order of 36% of *ADC* for practically all brain regions.

ACKNOWLEDGMENTS

The authors thank Drs. A.L. Sukstanskii and T. Tanoli for helpful discussion.

REFERENCES

1. Boesch C. MR and order in biological tissue. Special Issue NMR Biomed 2001;14.
2. van Zijl P, Le Bihan D. Diffusion tensor imaging and axonal mapping — state of the art. Special Issue NMR Biomed 2002;15.
3. Stejskal EO, Tanner JE. Spin diffusion measurements: spin echoes in the presence of a time-dependent field gradient. J Chem Phys 1965;42: 288–292.
4. Karlicek Jr RF, Lowe IJ. A modified pulsed gradient technique for measuring diffusion in the presence of large background gradients. J Magn Reson 1980;37:75–91.
5. Niendorf T, Dijkhuizen RM, Norris DG, van Lookeren Campagne M, Nicolay K. Biexponential diffusion attenuation in various states of brain tissue: implications for diffusion-weighted imaging. Magn Reson Med 1996;36:847–857.
6. Assaf Y, Cohen Y. Non-mono-exponential attenuation of water and N-acetyl aspartate signals due to diffusion in brain tissue. J Magn Reson 1998;131:69–85.
7. Assaf Y, Cohen Y. Structural information in neuronal tissue as revealed by q-space diffusion NMR spectroscopy of metabolites in bovine optic nerve. NMR Biomed 1999;12:335–344.
8. Assaf Y, Cohen Y. In vivo and in vitro bi-exponential diffusion of N-acetyl aspartate (NAA) in rat brain: a potential structural probe? NMR Biomed 1998;11:67–74.
9. Buckley DL, Bui JD, Phillips MI, Zelles T, Inglis BA, Plant HD, Blackband SJ. The effect of ouabain on water diffusion in the rat hippocampal slice measured by high resolution NMR imaging. Magn Reson Med 1999;41:137–142.
10. Pfeuffer J, Provencher SW, Gruetter R. Water diffusion in rat brain in vivo as detected at very large b values is multicompartmental. Magma 1999;8:98–108.
11. Mulkern RV, Zengingonul HP, Robertson RL, Bogner P, Zou KH, Gudbjartsson H, Guttmann CR, Holtzman D, Kyriakos W, Jolesz FA, Maier SE. Multi-component apparent diffusion coefficients in human brain: relationship to spin-lattice relaxation. Magn Reson Med 2000;44:292–300.
12. Mulkern RV, Vajapeyam S, Robertson RL, Caruso PA, Rivkin MJ, Maier SE. Biexponential apparent diffusion coefficient parametrization in adult vs newborn brain. Magn Reson Imag 2001;19:659–668.
13. Clark CA, Le Bihan D. Water diffusion compartmentation and anisotropy at high b values in the human brain. Magn Reson Med 2000;44: 852–859.
14. Inglis BA, Bossart EL, Buckley DL, Wirth 3rd ED, Mareci TH. Visualization of neural tissue water compartments using biexponential diffusion tensor MRI. Magn Reson Med 2001;45:580–587.
15. Yoshiura T, Wu O, Zaheer A, Reese TG, Sorensen AG. Highly diffusion-sensitized MRI of brain: dissociation of gray and white matter. Magn Reson Med 2001;45:734–740.
16. Stanisz GJ, Szafer A, Wright GA, Henkelman RM. An analytical model of restricted diffusion in bovine optic nerve. Magn Reson Med 1997; 37:103–111.
17. Ke Y, Cohen BM, Lowen S, Hirashima F, Nassar L, Renshaw PF. Biexponential transverse relaxation (T(2)) of the proton MRS creatine resonance in human brain. Magn Reson Med 2002;47:232–238.
18. Le Bihan D, Van Zijl P. From the diffusion coefficient to the diffusion tensor. NMR Biomed 2002;15:431–434.
19. Sehy JV, Ackerman JJ, Neil JJ. Evidence that both fast and slow water ADC components arise from intracellular space. Magn Reson Med 2002;48:765–770.
20. Chin CL, Wehrli FW, Hwang SN, Takahashi M, Hackney DB. Biexponential diffusion attenuation in the rat spinal cord: computer simulations based on anatomic images of axonal architecture. Magn Reson Med 2002;47:455–460.
21. van der Weerd L, Melnikov SM, Vergeldt FJ, Novikov EG, Van As H. Modelling of self-diffusion and relaxation time NMR in multicompartment systems with cylindrical geometry. J Magn Reson 2002;156:213–221.
22. Sukstanskii AL, Yablonskiy DA. Effects of restricted diffusion on MR signal formation. J Magn Reson 2002;157:92–105.
23. Latour LL, Svoboda K, Mitra PP, Sotak CH. Time-dependent diffusion of water in a biological model system. Proc Natl Acad Sci USA 1994; 91:1229–1233.
24. Szafer A, Zhong J, Gore JC. Theoretical model for water diffusion in tissues. Magn Reson Med 1995;33:697–712.
25. Ford JC, Hackney DB, Alsop DC, Jara H, Joseph PM, Hand CM, Black P. MRI characterization of diffusion coefficients in a rat spinal cord injury model. Magn Reson Med 1994;31:488–494.
26. Ford JC, Hackney DB, Lavi E, Phillips M, Patel U. Dependence of apparent diffusion coefficients on axonal spacing, membrane permeability, and diffusion time in spinal cord white matter. J Magn Reson Imag 1998;8:775–782.
27. Yablonskiy DA, Sukstanskii AL, Leawoods JC, Gierada DS, Bretthorst GL, Lefrak SS, Cooper JD, Conradi MS. Quantitative in vivo assessment of lung microstructure at the alveolar level with hyperpolarized 3He diffusion MRI. Proc Natl Acad Sci USA 2002;99:3111–3116.
28. Yablonskiy DA, Ackerman JJH, Raichle ME. Coupling between changes in human brain temperature and oxidative metabolism during prolonged visual stimulation. Proc Natl Acad Sci USA 2000;97:7603–7608.
29. Tanner JE. Transient diffusion in a system partitioned by permeable barriers. Application to NMR measurements with a pulsed field gradient. J Chem Phys 1978;69:1748–1754.
30. Kuchel PW, Durrant CJ. Permeability coefficients from NMR q-space data: models with unevenly spaced semi-permeable parallel membranes. J Magn Reson 1999;139:258–272.
31. Shimony JS, McKinstry RC, Akbudak E, Aronovitz JA, Snyder AZ, Lori NF, Cull TS, Conturo TE. Quantitative diffusion-tensor anisotropy brain MR imaging: normative human data and anatomic analysis. Radiology 1999;212:770–784.
32. Lee JH, Springer Jr CS. Effects of equilibrium exchange on diffusion-weighted NMR signals: the diffusigraphic "shutter-speed." Magn Reson Med 2003;49:450–458.